Comparison of several classical density functional theories for the adsorption of flexible chain molecules into cylindrical nanopores

S. P. Hlushak,[1,2,a)] P. T. Cummings,[1,3] and C. McCabe[1,4]
[1]*Department of Chemical and Biomolecular Engineering, Vanderbilt University, Nashville, Tennessee 37235, USA*
[2]*Institute for Condensed Matter Physics, Svientsitskoho 1, 79011 Lviv, Ukraine*
[3]*Center for Nanophase Materials Sciences, Oak Ridge National Laboratory, Oak Ridge, Tennessee 37831, USA*
[4]*Department of Chemistry, Vanderbilt University, Nashville 37235, USA*

(Received 17 September 2013; accepted 26 November 2013; published online 17 December 2013)

Adsorption of flexible oligomers into narrow cylindrical pores has been studied by means of several versions of classical density functional theory (CDFT) and Monte Carlo simulation. The adsorption process is interesting to study due to the competition between the entropic depletion of oligomers from the pores and the wall–oligomer attraction. It is also challenging to describe using current CDFTs, which tend to overestimate the amount of the adsorbed fluid. From a comparison of several different CDFT approaches, we find that this is due to the assumption of ideal or freely jointed chain conformations. Moreover, it is demonstrated that it is impossible to obtain a reasonable description of the adsorption isotherms without taking into account accurate contact values in the distribution functions describing the structure of the reference monomer fluid. At low densities, more accurate result are obtained in comparison with Monte Carlo simulation data when accurate contact values are incorporated into the theory rather than the more commonly used hard-sphere contact value. However, even the CDFT with accurate contact values still overestimates the amount of the adsorbed fluid due to the ideal or freely jointed chain approximation, used for the description of chain conformations in most CDFT approaches. We find that significant improvement can achieved by employing self-consistent field theory, which samples self-avoiding chain conformations and decreases the number of possible chain conformations, and, consequently, the amount of the adsorbed fluid. [http://dx.doi.org/10.1063/1.4843655]

I. INTRODUCTION

Adsorption of small molecules into porous materials plays an important role in many branches of science, including separations using adsorbents and membranes, catalysis, small molecule storage, and surface science.[1–4] Successful characterization of the pore and the thermodynamic and physical properties of the confined fluid would provide a better understanding of the adsorption process and lead to improvements in the large-scale application of adsorption technology.

In recent years, statistical mechanical approaches have increasingly become the theoretical method of choice for understanding and predicting adsorption phenomena.[5] Among these methods, molecular simulation plays an important role due to the high level of atomistic detail and transparency of the results it provides. Decades of exponential increases in computer power, combined with equally or larger increases in computational efficiency enabled by advances in algorithms, has allowed molecular simulation to become the almost universal modeling approach. Simulation, however, will not be able to fully replace analytical methods, in part because significant progress has yet to be made to make simulation facile for modeling problems spanning multiple time and length scales. Moreover, the understanding of both simulation and experimental results often requires interpretation, which is accomplished with the help of theoretical tools that are either analytically solvable or solved numerically many orders of magnitude faster than direct simulations can be performed.

CDFT is the primary theoretical tool for studying inhomogeneous systems (e.g., fluids at interfaces and in pores and the interphase between two fluid phases). CDFT approaches are increasingly being used for the description of adsorption processes and interfacial phenomena.[6] The performance gain over simulation is especially noticeable when the effective dimensionality of the problem can be reduced by exploiting the symmetry of the system, e.g., when the fluid is near a flat wall, its density depends only on the distance from the wall and not on the other two coordinates, resulting in a one-dimensional problem. However, the accuracy and robustness of CDFT depend on the knowledge of the analytic free-energy functionals and bulk-fluid correlation functions required as input to the theory. Often the lack of these important components forces investigators to use oversimplifications in the formulation of the CDFT, thus reducing the accuracy of the approach. Moreover, due to technical difficulties, the application of CDFT is typically limited to one-dimensional problems of the adsorption of simple fluids into slit pores. Among the studies that use multi-dimensional implementations of CDFT,[7–18] we highlight those that utilize Fourier transforms to integrate the convolution integrals.[10–14,17] The latter are encountered in the formulation of the fundamental measure theory[19] (FMT) and its variants,[20,21] where weighted particle densities are

a)Electronic mail: stepan.hlushak@gmail.com

calculated as convolutions of the weight functions with the particle density function, and in the Taylor expansion of the free energy functional, where the direct correlation function is convoluted with the density difference. Besides offering performance advantages,[10–12,14] the Fourier-space implementations tend to be simpler. This is partially a result of the fact that the correlation functions obtained from integral equations theories tend to have forms that are expressed much more simply in Fourier[14] space than in real space.[22–24]

In this study, we propose several modifications to basic CDFT and examine the adsorption of oligomers into narrow infinitely long pores of arbitrary cross-section geometry. Our aim is to investigate how well CDFT theory is suited for the description of the adsorption of flexible chain molecules. We demonstrate that the accuracy of the theory can be enhanced through the use of accurate bulk-fluid direct correlation functions and contact values, calculated using a first-order mean spherical approximation (FMSA).[25]

The FMSA theory[25] is a simpler variant of the mean spherical approximation[26–32] (MSA), that has an analytic solution for a range of model fluids, including square-well and square-shoulder (i.e., repulsive square well) fluids,[23,33–35] Yukawa and multi-Yukawa,[36,37] Kihara, Lennard–Jones,[34] and, additionally, a variety of discrete potentials fluids.[24] While the FMSA is a simpler theory, it is only slightly less accurate than the full MSA solution, and in contrast to the latter, is solvable at any thermodynamic condition.[38] Its simplicity and analyticity, however, make it attractive for use in different related approaches, such as CDFT,[14,36,39–46] augmented perturbation theory,[47] and other advanced approximations.[37] The FMSA is used here to calculate the thermodynamic and structural properties of the bulk homogeneous fluid.

II. MODEL AND THEORY

A. Model

We consider a fluid of chain molecules composed of m tangentially bonded spherical segments that interact through a hard-sphere plus a square-well (SW) potential,

$$u_{sw}(r) = \begin{cases} \infty, & r < \sigma \\ -\varepsilon, & \sigma \le r < (1+\lambda)\sigma \\ 0, & r \ge (1+\lambda)\sigma. \end{cases} \quad (1)$$

The length of the bond between the consecutive segments is equal to the segment diameter, σ, and there is no angular constraint between the neighboring bonds. The chain molecules are therefore freely jointed in that the segments can freely slide over the surface of one another, unless another segment is encountered.

The molecules are confined in cylindrical pores with hard and attractive walls, which are modeled by an external potential V_{ext} acting on each monomer of the chain molecules. In the case of pores of radius R with hard walls, the potential reads

$$v(r) = \begin{cases} \infty, & r > R \\ 0, & \text{otherwise}, \end{cases} \quad (2)$$

where r is the distance from the centre of the pore. For square-well attractive pores, the potential is given by

$$v(r) = \begin{cases} \infty, & r > R, \\ -\varepsilon_{wall}, & R - \lambda_{wall}\sigma < r \le R, \\ 0, & \text{otherwise}. \end{cases} \quad (3)$$

Here, ε_{wall} is the depth of the wall potential well and λ_{wall} is the width of the well in units of σ.

To test the CDFT approaches proposed we have considered two different pore sizes, corresponding to pore radii of 2.0σ and 3.0σ, as well as the effect of variations in the strength of the wall-fluid attraction with the following wall-fluid well depths considered: $\varepsilon_{wall} = 0$, $\varepsilon_{wall} = \varepsilon$ and $\varepsilon_{wall} = 2\varepsilon$, which correspond to repulsive, slightly attractive, and attractive walls, respectively. The width of the wells in all cases is $\lambda_{wall} = 1$. The pore model is similar to that used in our previous work,[14] where the adsorption of SW monomers into cylindrical pores was studied.

B. Polymeric density functional theory

The first density-functional description of chain molecules that we consider is based on the polymeric DFT theory of Yu and Wu.[48] According to the formalism of the theory, the local number density of the chains $\rho_M(\mathbf{R})$ depends on the positions of all segments, $\mathbf{R} = \{\mathbf{r}_1, \mathbf{r}_2, \ldots, \mathbf{r}_M\}$. The connectivity between the segments is imposed by an intramolecular bonding potential $V_b(\mathbf{R}) = \sum_{i=1}^{M-1} v_b(|\mathbf{r}_{i+1} - \mathbf{r}_i|)$, where M is the number of segments in the chain. In order to ensure connectivity between the two segments, the bonding potential between the neighboring segments $v_b(r)$ is given by $\exp[-\beta v_b(r)] = \delta(r-\sigma)/(4\pi\sigma^2)$. Therefore, the full bonding potential $V_b(\mathbf{R})$ satisfies the condition

$$e^{-\beta V_b(\mathbf{R})} = \prod_{i=1}^{M-1} \frac{\delta(|\mathbf{r}_{i+1} - \mathbf{r}_i| - \sigma)}{4\pi\sigma^2}. \quad (4)$$

The total number density of segments is defined as[48]

$$\rho(\mathbf{r}) = \sum_{i=1}^{M} \rho_i(\mathbf{r}), \quad (5)$$

where $\rho_i(\mathbf{r})$ is the local density of the segment number i,

$$\rho_i(\mathbf{r}) = \int d\mathbf{R}\delta(\mathbf{r} - \mathbf{r}_i)\rho_M(\mathbf{R}). \quad (6)$$

The free energy functional is expressed[48] as the sum of ideal, F_{id},

$$\beta F_{id}[\rho_M(\mathbf{R})] = \int d\mathbf{R}\rho_M(\mathbf{R})(\ln(\rho_M(\mathbf{R})) - 1) + \beta \times \int d\mathbf{R}\rho_M(\mathbf{R})V_b(\mathbf{R}) \quad (7)$$

and excess, F_{ex}, terms. The latter term is the sum of the hard-sphere contribution, F_{hs}, the contribution arising from the chain connectivity, F_c, and contribution accounting for attractive square-well interactions, F_{at}. Both F_{hs} and F_c can be

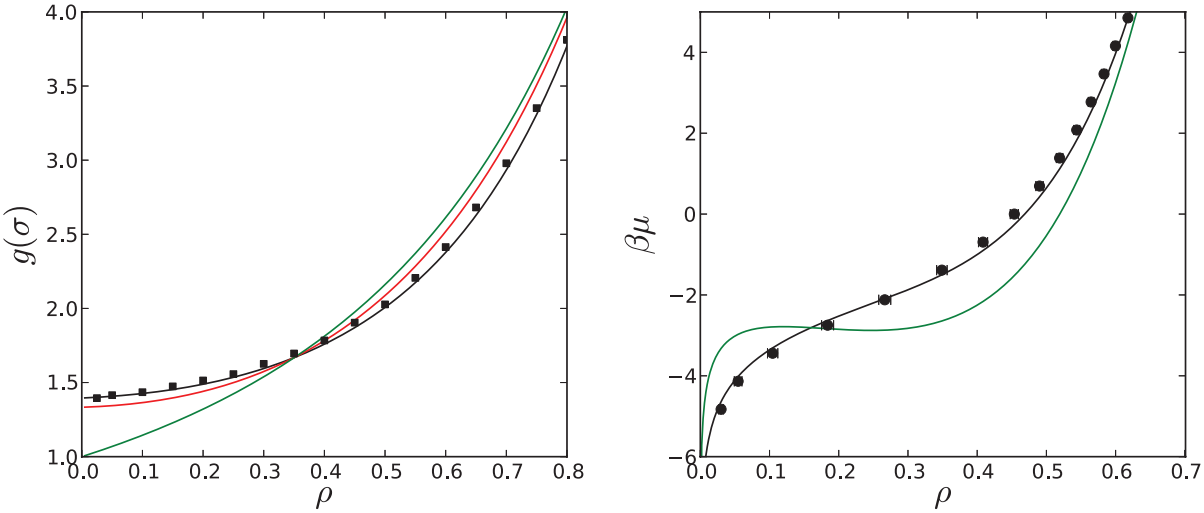

FIG. 1. Left: Density dependence of the contact value of the radial distribution function of the monomer SW fluid with $\lambda = 0.5$ and $\epsilon = 1$ at $T^* = 3$. The black line is the exponential approximation, the red line is the conventional approach, i.e., $g(\sigma) = g_{hs}(\sigma) + g_1(\sigma)$, and the green line show the hard-sphere contact value. The symbols are simulation results of Tavares[51] for the contact value of the SW fluid. Right: Chemical potential of a 6-mer made of SW segments in the fluid composed of similar 6-mers at $T^* = 3$ and different densities. The black line denotes the prediction of the homogeneous fluid theory with contact values from the exponential approximation, while the green line represents predictions of the homogeneous fluid theory with the hard-sphere contact value. The symbols denote results of the grand canonical MC.

written as

$$\beta F_\alpha [\rho(\mathbf{r})] = \int d\mathbf{r} \Phi_\alpha(\mathbf{r}), \tag{8}$$

where $\alpha = hs$ or c and Φ_α is the relevant free energy density. The hard-sphere excess free energy density results from fundamental measure theory,[19] viz.,

$$\Phi_{hs} = -n_0 \ln(1-n_3) + \frac{n_1 n_2 - \mathbf{n}_1 \cdot \mathbf{n}_2}{1-n_3} + n_2^3 (1-\xi^2)^3 \frac{n_3 + (1-n_3)^2 \ln(1-n_3)}{36\pi n_3^2 (1-n_3)^2}. \tag{9}$$

The chain connectivity contribution is calculated from Wertheim's thermodynamic perturbation theory[49] as

$$\Phi_c = \frac{1-M}{M} n_0 \zeta \ln g[\rho(\mathbf{r})]. \tag{10}$$

In the above $n_i, i = 0, 1, 2, 3$ and $\mathbf{n}_i$, $i = 1, 2$ are the weighted densities that are given as convolutions of the total segment density with corresponding weight functions from fundamental measure theory. For their definitions and evaluation, see Refs. 19 and 50 and Appendix A of Ref. 10. The quantities ξ and ζ are defined as $\xi = |\mathbf{n}_2(\mathbf{r})| / n_2(\mathbf{r})$ and $\zeta = 1 - \mathbf{n}_2 \cdot \mathbf{n}_2 / n_2^2$, and $g(\sigma)$ is the contact value of the radial distribution function of the square-well fluid. The latter, when the exponential approximation is used, is given by

$$g[\rho(\mathbf{r})] = g_{hs}[\rho(\mathbf{r})] \exp(g_1(n_3(\mathbf{r}))), \tag{11}$$

where

$$g_{hs}[\rho(\mathbf{r})] = \frac{1}{1-n_3} + \frac{n_2 \sigma \zeta}{(1-n_3)^2} + \frac{(n_2\sigma)^2 \zeta}{72(1-n_3)^3}, \tag{12}$$

is the contact value of the hard-sphere radial distribution function, and

$$g_1(\eta) = \sum_{i=0}^{2} \left(A_i(\eta) f_i^{(A)}(\eta) + B_i(\eta) f_i^{(A)}(\eta) \right), \tag{13}$$

is the excess (to hard-sphere) contact value for square-well fluid obtained from the first-order mean-spherical approximation (FMSA).[33] The functions $A_i(\eta)$, $B_i(\eta)$, $f_i^{(A)}(\eta)$, and $f_i^{(B)}(\eta)$ are defined by Eq. (6) of Ref. 33 and are presented in the Appendix. The quality of the contact value in the exponential approximation can be deduced from Fig. 1 (left plot), where comparisons are made with the simulation results of Tavares *et al.*[51] From the figure, we can see that the agreement between the results of the simulations and the exponential approximation is excellent and that the contact value of the FMSA theory without the exponential approximation ($g(\sigma) = g_{hs}(\sigma) + g_1(\sigma)$) is only slightly less accurate.

The free-energy term responsible for the incorporation of the square-well attraction is approximated by expansion of the functional around some reference total segment number density ρ_{ref} truncated to second order:[52,53]

$$\beta F_{at}[\rho(\mathbf{r})] = \beta F_{at}(\rho_{ref}) + \beta \mu_{at}(\rho_{ref}) \int d\mathbf{r}_1 (\rho(\mathbf{r}_1) - \rho_{ref}) - \frac{1}{2} \int d\mathbf{r}_1 d\mathbf{r}_2 c_{att}(|\mathbf{r}_1 - \mathbf{r}_2|; \rho_{ref}) \times (\rho(\mathbf{r}_1) - \rho_{ref})(\rho(\mathbf{r}_2) - \rho_{ref}), \tag{14}$$

where $F_{at}(\rho_{ref})$, $\mu_{at}(\rho_{ref})$, and $c_{at}(\mathbf{r}_1, \mathbf{r}_2; \rho_{ref})$ are the excess free energy, chemical potential and direct correlation function (DCF) (respectively) of the bulk square-well fluid at a total segment density ρ_{ref}. In the current work, these quantities are also evaluated using the FMSA.[22,23,33]

There are several possible ways of choosing the method for calculating the reference segment number density (ρ_{ref}).

One of the simplest and most commonly used is to set it equal to the density ρ_b of the bulk fluid that is assumed to be in equilibrium with the inhomogeneous one. However, such an approach can lead to inaccuracies when the density of the inhomogeneous fluid is significantly different from the bulk one and the temperature is sufficiently low. This is because the expansion in Eq. (14) is inaccurate for significant density differences that occur for fluids confined in highly attractive pores, and becomes increasingly important when compared to the hard-sphere contribution as temperature is lowered. To overcome this problem, we recently implemented[14] the reference fluid density functional approach of Gillespie *et al.*,[54] and applied it to describe the adsorption of the square-well and multi-Yukawa fluids into narrow nanopores. However, in the present work, in order to simplify and lower the cost of the calculations, we employ only the bulk density expansion approach ($\rho_{ref} = \rho_b$). This should be sufficiently accurate at the high temperatures studied: all calculations were performed at a temperature of $T^* = k_BT/\epsilon = 3$ (where k_B is Boltzmann's constant), and seems to be sufficiently high to justify the application of the bulk density expansion approach. As it will be shown later, the contribution from the intermolecular attraction is not the main shortcoming in the CDFT approaches considered that requires improvement.

The equilibrium properties are obtained by minimizing the functional

$$\Omega = F\left[\rho_M(\mathbf{R}), \rho_M(\mathbf{r})\right] + \int d\mathbf{R}\rho(\mathbf{R})\left(v_{ext}(\mathbf{R}) - \mu_M\right), \tag{15}$$

with respect to the chain density profile $\rho_M(\mathbf{R})$. In the above equation, the μ_M is the chemical potential of the bulk chain fluid:

$$\mu_M(\rho_b) = \mu_{M,re}(\rho_b) + M\mu_{at}(\rho_b), \tag{16}$$

where $\mu_{M,re}$ is a chemical potential of the chain without square-well attraction between segments and μ_{at} is the excess to hard-sphere chemical potential of the square-well fluid. Equation (16) defines the relation between the chemical potential and the total segment density, ρ_b, of the uniform bulk fluid. $\mu_{M,re}$ is given by

$$\beta\mu_{M,re}(\rho_b) = \ln\left(\frac{\rho_b}{M}\right) + \beta M\mu_{hs}(\rho_b) + (1-M) \times \left[\ln g_b(\sigma) + \rho_b\frac{\partial \ln g_b(\sigma)}{\partial\rho_b}\right], \tag{17}$$

where $\mu_{hs}(\rho_b)$ and $g_b(\sigma)$ are the excess chemical potential of hard spheres and the contact value of the radial distribution function of square-well fluid at bulk density ρ_b, respectively. The analytic expressions for the derivative of the contact value $\partial \ln g_b(\sigma)/\partial\rho_b$ are presented in the Appendix.

Minimization of the grand potential (15) yields the Euler–Lagrange equation

$$\rho_M(\mathbf{R}) = \exp\left\{\beta\mu_M - \beta V_b(\mathbf{R}) - \beta\sum_{i=1}^{M}\Lambda_i(\mathbf{r}_i)\right\}, \tag{18}$$

where $\Lambda_i(\mathbf{r}_i) = \delta F_{ex}/\delta\rho_i(\mathbf{r}_i) + v_i(\mathbf{r}_i)$, is an effective potential acting on individual segments. After using Eq. (6) to calculate the individual segment densities, Eq. (18) yields

$$\rho_i(\mathbf{r}) = \exp\left\{\beta\mu_M - \beta\Lambda_i(\mathbf{r})\right\} G_i(\mathbf{r}) G_{M-i+1}(\mathbf{r}), \tag{19}$$

where $G_i(\mathbf{r})$ is determined from the recurrence relation

$$G_i(\mathbf{r}) = \int d\mathbf{r}_{i-1}\exp\left\{-\beta\Lambda_i(\mathbf{r}_{i-1})\right\}\frac{\delta\left(|\mathbf{r}_{i-1}-\mathbf{r}|-\sigma\right)}{4\pi\sigma^2} \times G_{i-1}(\mathbf{r}_{i-1}), \quad i = 2, 3, \ldots, M \tag{20}$$

with $G_1(\mathbf{r}) = 1$, and the total segment density is given by

$$\rho(\mathbf{r}) = \sum_i \rho_i(\mathbf{r}). \tag{21}$$

The three-dimensional Fourier transform of the DCF $c_{att}(|\mathbf{r}_1 - \mathbf{r}_2|;\rho_b)$, that is used to evaluate expansion (14), reads

$$\tilde{c}_{att}(k;\rho) = \frac{4\pi}{k}\int_0^\infty dr\sin(kr)\, r c_{att}(r;\rho) = \frac{2\pi}{ik}\left[\hat{c}_{att}(-ik\sigma;\rho) - \hat{c}_{att}(ik\sigma;\rho)\right], \tag{22}$$

where

$$\hat{c}_{att}(s;\rho) = \beta\varepsilon(1-\eta)^4\sigma^2\hat{Q}_0^2(-s)\,\hat{p}(s) \tag{23}$$

is the Laplace transform of the DCF. Expressions for $c_{att}(|\mathbf{r}_1 - \mathbf{r}_2|;\rho_b)$, $\hat{Q}_0(s)$ and $\hat{p}(s)$ have been presented in previous work.[14,22,23]

The density along the pore axis is assumed to be uniform. The values of the density in the perpendicular cross-section of the pore are stored on a rectangular grid. Thus, the pore is modeled as an infinite cylindrical hole with hard walls.

C. Interfacial SAFT density functional theory

Another CDFT approach examined here is based on the density functional theory employed in the interfacial statistical associating fluid theory (iSAFT) proposed by Chapman and co-workers.[55,56] We utilize the iSAFT DFT expressions for the functional form of the contribution to the free energy due to chain connectivity, but use the FMSA-derived contributions for the attractive interactions.

The derivation of iSAFT DFT chain term starts from the thermodynamics of a reference fluid of associating monomers with two association points on the surface, which in the limit of complete association form chains. The thermodynamics is described in terms of Wertheim's first order thermodynamic perturbation theory (TPT1).[49] The resulting expressions for the density profiles are similar to the expressions obtained in the polymeric DFT theory of Yu and Wu,[48] because they involve the calculation of recurrence relations similar to those in Eq. (20),

$$I_j(\mathbf{r}_j) = g'\left[\rho(\mathbf{r}_j)\right]^{1/2}\int d\mathbf{r}_{j-1} I_{j-1}(\mathbf{r}_{j-1})\, g'\left[\rho(\mathbf{r}_{j-1})\right]^{1/2} \times \frac{\delta\left(|\mathbf{r}_{i-1}-\mathbf{r}_j|-\sigma\right)}{4\pi\sigma^2} e^{D_{j-1}(\mathbf{r}_{j-1})-\beta v_{j-1}(\mathbf{r}_j)}, \tag{24}$$

with $I_1(\mathbf{r}_1) = 1$.

The expression for the density of monomer i is only slightly different from the corresponding expression used in

polymeric DFT (19). For homonuclear chains:

$$\rho_j(\mathbf{r}_j) = \exp\{\beta\mu_M + D_j(\mathbf{r}_j) - \beta v_j(\mathbf{r}_j)\} \times I_j(\mathbf{r}_j) I_{M-j+1}(\mathbf{r}_j), \quad (25)$$

where

$$D_i(\mathbf{r}_i) = \frac{1}{2}\sum_{j=1}^{M}\sum_{k}^{\{neigh.\}}\int d\mathbf{r}_1 \rho_k(\mathbf{r}_1)\frac{\delta \ln g_{jk}[\rho(\mathbf{r}_1)]}{\delta\rho_i(\mathbf{r})} - \beta\frac{\delta F_{hs}[\rho(\mathbf{r})]}{\delta\rho_i(\mathbf{r})} - \beta\frac{\delta F_{att}[\rho(\mathbf{r})]}{\delta\rho_i(\mathbf{r})} \quad (26)$$

contains derivatives of several parts of the free energy functional, and the second summation is over the neighboring segments of k.

The key difference between the chain terms of iSAFT DFT and polymeric DFT is in the way the contact value of the reference fluid is incorporated. Since we consider only homonuclear chains, the contact value of the radial distribution function of the reference fluid is independent of the monomer position in the chain and is given by

$$g_{ik}[\rho(\mathbf{r})] = g'[\rho(\mathbf{r})] = g'_{hs}[\rho(\mathbf{r})]\exp(g_1(\bar{s}_3(\mathbf{r}))), \quad (27)$$

where g_1 is given by (13) and

$$g'_{hs}[\rho(\mathbf{r})] = \frac{1}{1-\bar{s}_3} + \frac{3\sigma}{2}\frac{\bar{s}_2}{(1-\bar{s}_3)^2} + \frac{\sigma^2}{2}\frac{\bar{s}_2^2}{(1-\bar{s}_3)^3}, \quad (28)$$

$$\bar{s}_i(\mathbf{r}_1) = \frac{1}{8\sigma^{3-i}}\int_{|\mathbf{r}_1-\mathbf{r}_2|<\sigma} d\mathbf{r}_2\rho(\mathbf{r}_2), \quad i = 0, 1, 2, 3. \quad (29)$$

These expressions are different than those (Eqs. (11)–(13)) of the polymeric DFT theory, since they are composed of different weighted densities.

In this work, all the other reference monomer fluid properties, such as excess contact value, $g_1(r)$, and contributions to the thermodynamics from the attractive interactions are obtained from the FMSA theory, similarly, as was done for the polymeric DFT theory (see Sec. II B).

The main motivation for comparison of the iSAFT DFT and polymeric DFT is different functional expressions for the contact value employed by the two theories. As will be shown later, CDFT is very sensitive to the quality of the contact value used in the chain connectivity contribution. Therefore, different functional expression of the contact value used by the two theories will lead to different descriptions of the inhomogeneous fluid.

The CDFT approaches described thus far are quite robust and computationally cheap methods for estimation of equilibrium density profiles and adsorption isotherms of confined chain fluids. As in our previous work,[14] all the convolution integrals, arising in the implementation of the fundamental measure theory (i.e., Eq. (8)), functional Taylor expansion (14) and the recurrence relations (20) and (24), were integrated in Fourier space, which yields a significant increase in computational performance[10] when compared to real-space approaches. Nevertheless, the approaches have also a downside, which will be discussed in Sec. II D.

D. Self-consistent field theory

In both of the CDFT approaches described thus far the sampled chain conformations are ideal, which leads to inadequate predictions for the structure of the chain fluids that becomes progressively less accurate as chain length increases. To avoid the ideal chain approximation we employed single-chain simulations to sample conformations, as was recently proposed in a self-consistent field theory (SCFT) approach described by Bryk and MacDowell.[57] According to Ref. 57, the density of a particular chain conformation can be rewritten as

$$\rho(\mathbf{R}) = P(\mathbf{R})\exp\left\{\beta\mu - \beta\sum_{i=1}^{M}\Lambda_i(\mathbf{r}_i)\right\},$$

where $P(\mathbf{R})$ is a probability of a conformation given by monomer position vector $\mathbf{R} = \{r_1, \cdots, r_M\}$, and the exponent is the Boltzmann factor of the chain potential energy in the effective external field given by $\mu - \Lambda(\mathbf{r})$. The segment density is then obtained as an average over the intramolecular chain conformation described by $P(\mathbf{R})$,

$$\rho(\mathbf{r}) = \exp(\beta\mu)\left\langle\sum_{i=1}^{M}\delta(\mathbf{r}-\mathbf{r}_i)\exp\left\{-\beta\sum_{i=1}^{M}\Lambda_i(\mathbf{r}_i)\right\}\right\rangle_{intra}. \quad (30)$$

For ideal or freely-jointed chains the intramolecular probability reads

$$P(\mathbf{R}) = \exp\{-\beta V_b(\mathbf{R})\} = \frac{1}{4\pi\sigma^2}\prod_{i=1}^{M-1}\delta(|\mathbf{r}_i - \mathbf{r}_{i+1}| - \sigma).$$

This clearly preserves the distance between the monomers, but does not prevent monomers in the same chain from overlapping. Thus, the generated conformations are not self-avoiding.

In our current implementation, we have generated a large table of chain conformations at the beginning of the iterative solution and used it to generate averages at each iteration. To gain better accuracy by employing the SCFT DFT, one has to sacrifice the numerical robustness offered by the recurrence relations (20) and (24). In the current implementation, they are efficiently calculated in Fourier space using the convolution theorem. Replacing them with an approach that evaluates realistic molecule conformations allows the introduction of different kinds of intramolecular bonding potentials, which could close the gap between the level of molecular detail in CDFT compared to Monte Carlo simulation approaches. Nevertheless, evaluating energies of the pre-generated chain conformation at every iteration is computationally demanding. It takes several minutes to converge for the SCFT DFT theory with 4×10^5 stored chain conformations, while similar PDFT and iSAFT theories converge in few seconds. Monte Carlo simulation of similar system runs for few hours. Incorporation of a more efficient solver could make CDFT approaches much more appealing for applications involving complex fluids and their mixtures, where traditionally only Monte Carlo simulation approaches have been used successfully.

E. Monte Carlo simulation

To test the theoretical predictions, we have performed configurationally biased grand canonical Monte Carlo (GCMC) simulations of the adsorption of two SW chain fluids, 6-mers and 12-mers, into cylindrical pores. For different bulk chemical potentials adsorption was simulated at $T^* = 3.0$, where $T^* = T/\epsilon$ is the dimensionless temperature and $\rho^* = \rho\sigma^3$ is the dimensionless density.

The selected temperature ($T^* = 3.0$) is supercritical for the studied model fluids, and, therefore, the vapor-liquid phase transition is not observed.

Configurationally biased Monte Carlo (CBMC) algorithms from Frenkel and Smit[58] were used with grand-canonical moves and an additional geometric constraint added to mimic a hard cylindrical pore. The code was tested by simulating adsorption of hard chains (without SW attraction) into hard cylindrical pores and comparing to published results.[11]

The GCMC simulations, performed at fixed temperature and chemical potential, result in a chemical potential versus average density dependence. This dependence was obtained for all pores including the case of the bulk fluid. The latter is simply the bulk fluid chemical potential and is compared to the prediction of the FMSA-based TPT1 theory in Fig. 1. The GCMC results are presented in the form of adsorption isotherms for different pore sizes in Figs. 2 and 3, and in the form of radial density profiles in Figs. 4 and 5 to illustrate the in-pore structure. The density profiles were sampled at specific average pore packing fractions ($\eta = 0.1$, 0.2 and 0.3). In order to obtain the corresponding input chemical potentials, the adsorption isotherm was interpolated and evaluated at the required average pore packing fractions. The obtained chemical potential was then used as an input into the subsequent simulations to determine the density profiles.

The volume of the simulation box was always $10^3\sigma^3$ for both the bulk and inhomogeneous systems, which implies that the pore length is different for pores of different width, while the volume remains constant. Thus, for example, the box size for a pore of radius of $R = 3\sigma$ was $6\sigma \times 6\sigma \times 27.8\sigma$.

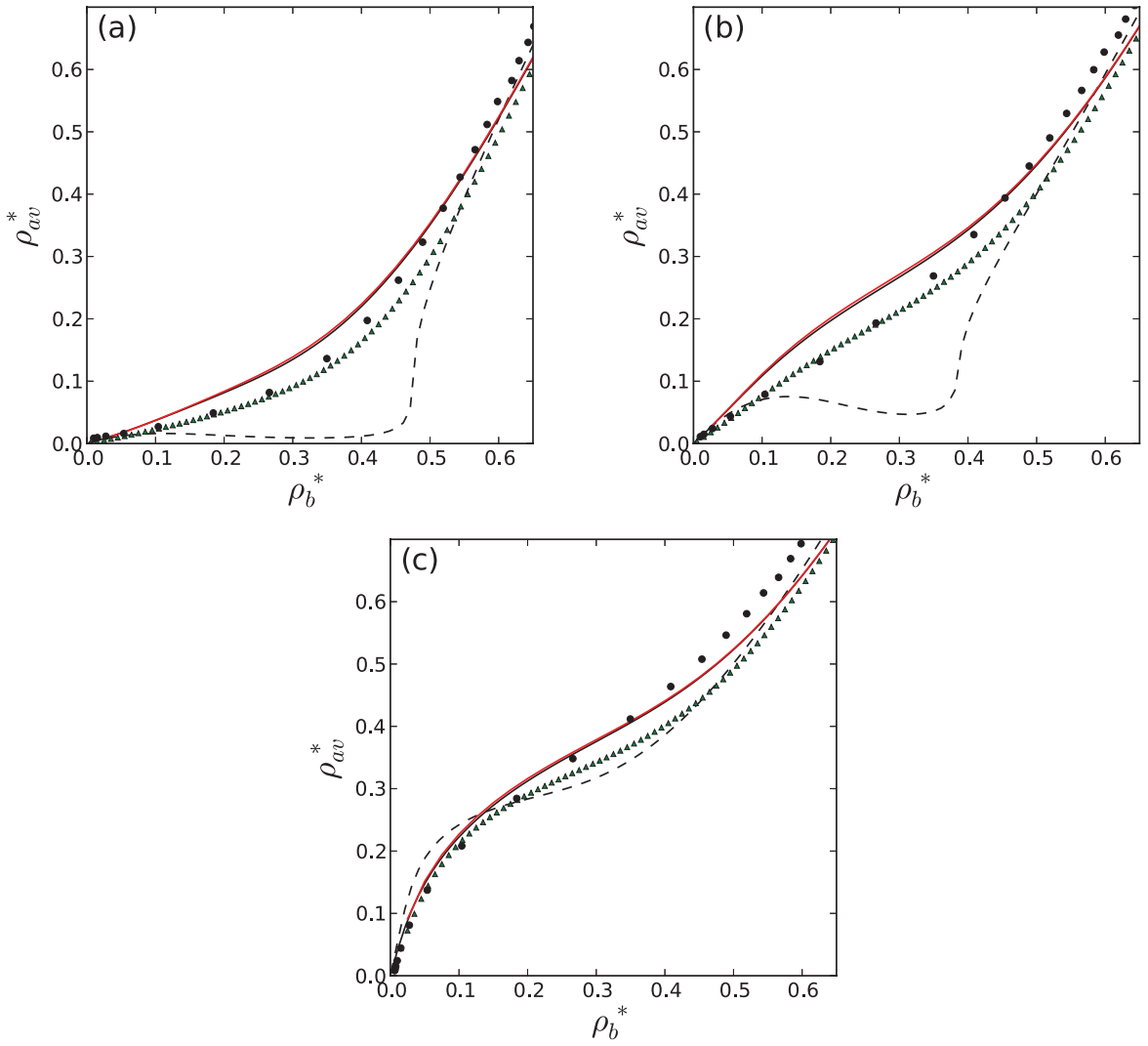

FIG. 2. Comparison of adsorption isotherms of 6-mers at $T^* = 3.0$ (average pore density vs. bulk density) for three different pores with $R^* = R/\sigma = 2.0$ and different wall-fluid attraction strength: (a) absence of any attraction (i.e., hard walls), (b) attractive wall ($\varepsilon_{wall} = \varepsilon$, $\lambda_{wall} = 1$), and (c) strongly attractive wall ($\varepsilon_{wall} = 2\varepsilon$, $\lambda_{wall} = 1$), obtained from the version of the polymeric DFT theory (black line), version of the iSAFT theory (red line), the version of the polymeric DFT theory with hard-sphere contact value (black dashed line), self-consistent field theory (green triangles), and GCMC simulations (black circles).

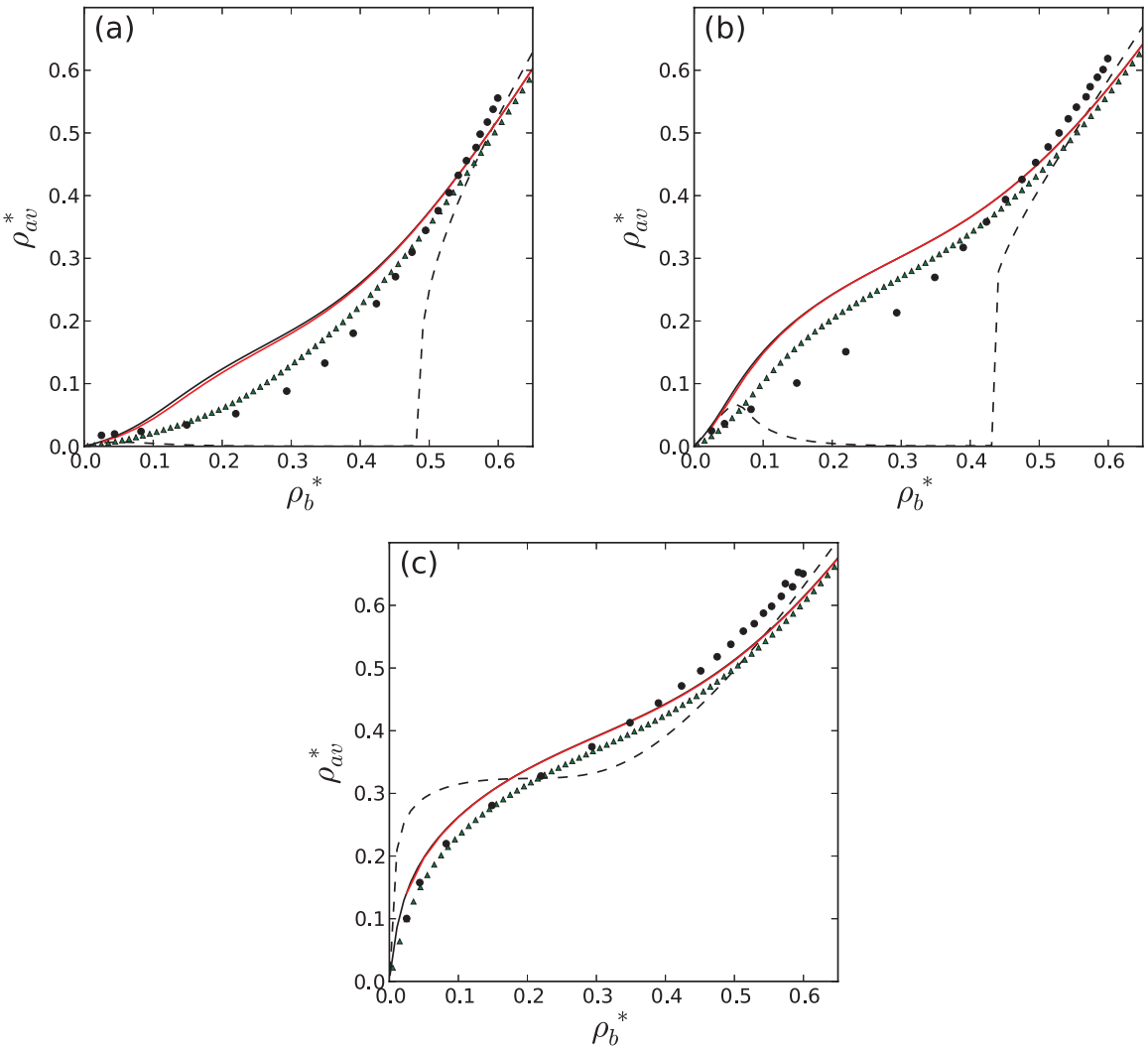

FIG. 3. The same as Fig. 2, but for 12-mers and pore with radius $R^* = R/\sigma = 3.0$.

Standard periodic boundary conditions were applied along the cylindrical pore axis.

A Monte Carlo step consisted of an attempt to displace a randomly selected molecule, an attempt to delete and regrow a randomly selected molecule and an attempt to insert or remove a randomly selected molecule, with probabilities of selecting a particular move: 10%, 40% and 50%, respectively.

1×10^7 Monte Carlo steps were performed to allow each system to reach equilibrium before production runs of at least 5×10^7 additional Monte Carlo steps were carried out. The average density of the fluid inside the pore and the radial density profiles were calculated by determining the number of particles and their radial distribution histogram inside the pore every 1000 steps and then averaging the summed values at the end of simulation.

III. RESULTS AND DISCUSSION

For the two chain fluids studied ($m = 6$ and $m = 12$), the monomers were selected to interact with each other according to the hard-sphere plus SW potential with width $\lambda = 0.5$ at fixed temperature $T^* = k_BT/\epsilon = 3$, and were confined in cylindrical pores with both hard and SW walls. The confined fluids are assumed to be in equilibrium with a similar bulk fluid. Pore adsorption isotherms and density profiles were calculated using the proposed CDFT approaches and GCMC simulation. The fluid density profiles, in our CDFT implementations, were discretized and stored on an equally spaced grid with a step size of 0.025σ in both directions. Similarly, the DCF of the fluid was stored on a Fourier-space grid, with each point of the grid corresponding to a particular k-vector.

The grid for the SCFT approach was not dense (step size: 0.05σ). This was dictated by the fact that the number of sampled single-chain conformations was limited by the available memory and was insufficient to obtain high quality in-pore density profiles. In order to present them graphically we have averaged every two points into one and presented them as symbols along with the Monte Carlo simulation profiles in Figs. 4 and 5. Nonetheless, the adsorption isotherms, or the average adsorbed densities, calculated using the SCFT appear to be of high quality (see Figs. 2 and 3).

For more details on our algorithms, the reader is directed to previous works,[11,14] in which the analytic expressions for the Fourier transforms of the weight functions and direct

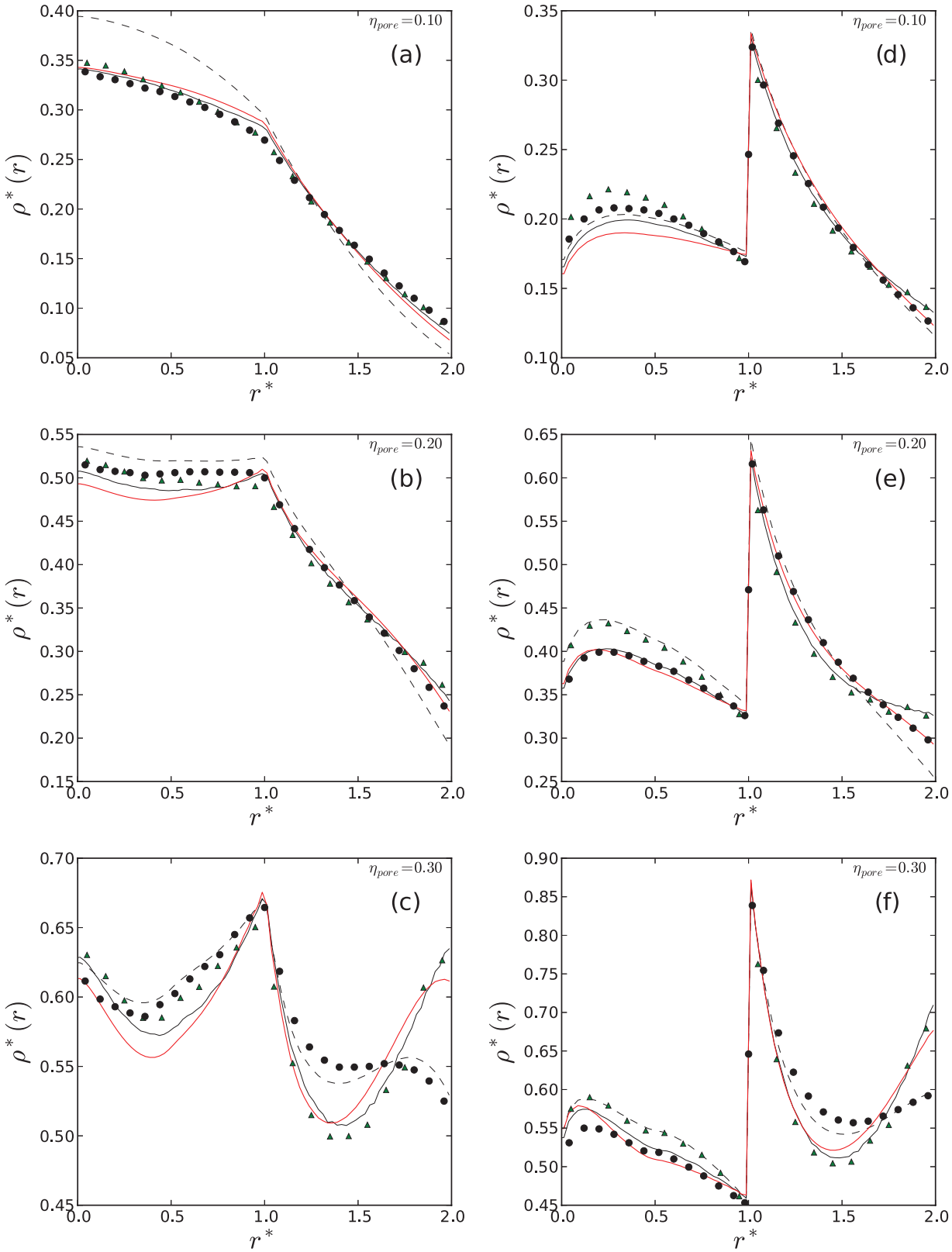

FIG. 4. Radial monomer density profiles ($r^* = r/\sigma$ is a distance from the centre of the pore) of 6-mers inside infinite cylindrical pore with $R^* = R/\sigma = 2.0$ at $T^* = 3.0$, and at three different average pore packing fractions: $\eta_{pore} = 0.1$, 0.2, and 0.3, and two different walls: hard wall (plots (a), (b), and (c)) and SW wall ($\varepsilon_{wall} = 2\varepsilon$ and $\lambda_{wall} = 1$) (plots (e), (f), and (g)). Black lines denote results of the version of the polymeric DFT theory with the contact value in the exponential approximation, red lines show results of the version of the iSAFT theory with the exponential contact value, while the black dashed lines denote results of the polymeric DFT approach with hard-sphere contact value. Symbols denote results of the MC simulation (black circles) and SCFT (green triangles).

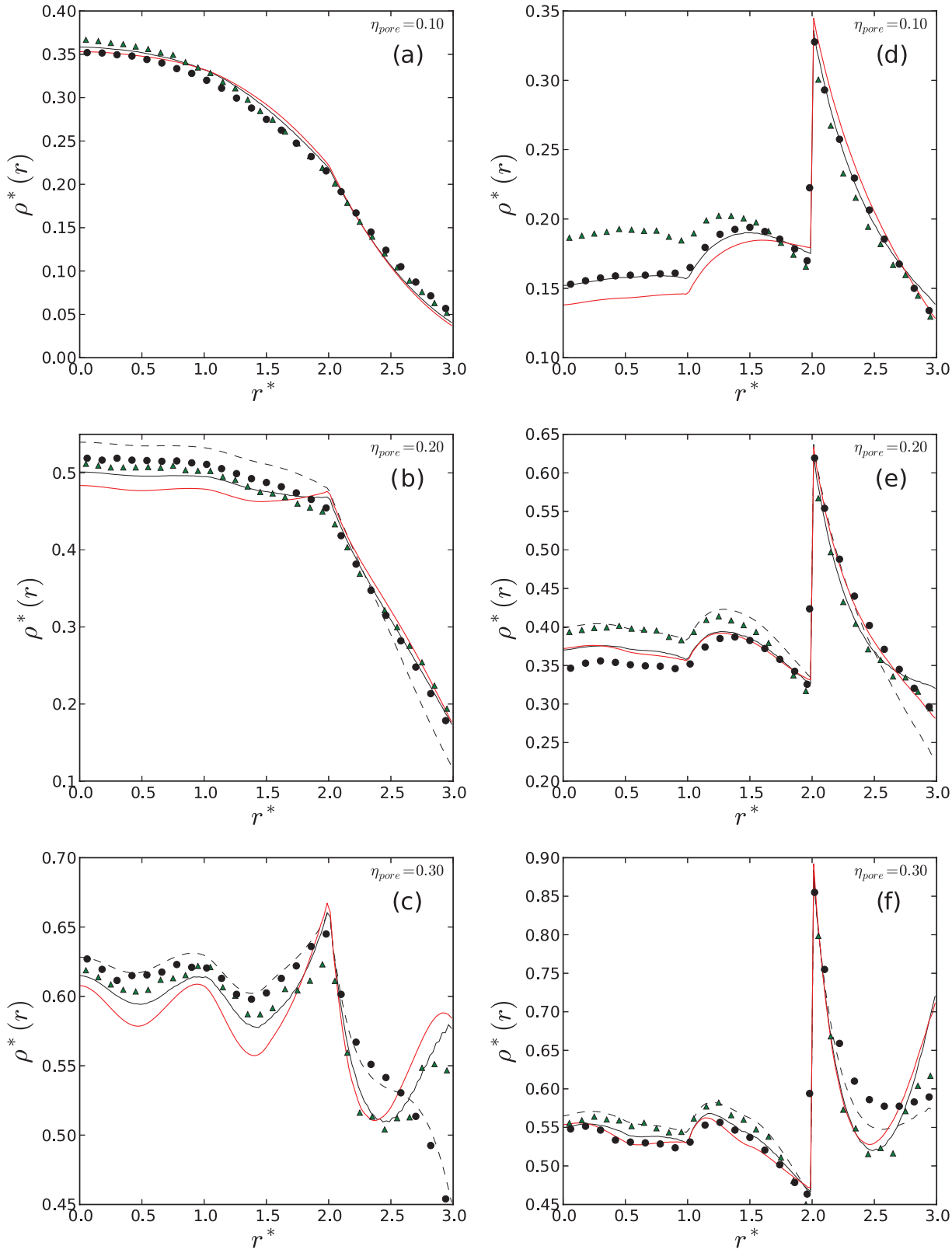

FIG. 5. The same as Fig. 4, but for 12-mers and pore with radius $R^* = R/\sigma = 3.0$.

correlation functions, together with analytic expressions for the thermodynamics are presented.

Before proceeding to the analysis of the CDFT results, we test the predictions of the corresponding homogeneous fluid theory. The homogeneous fluid theory is central to CDFT since it is used to estimate the thermodynamic (free energy and chemical potentials) and structural properties (DCF and contact values) of the bulk and adsorbed fluids. The chemical potential, for example, is calculated for both the bulk and adsorbed fluids. The chemical potential of the bulk fluid is

given by Eq. (16) at the bulk fluid density, ρ_b and enters the Euler-Lagrange equation (18). For the adsorbed fluid only the attractive part of the chemical potential is utilized (see Eq. (14)), which corresponds to some hypothetical homogeneous fluid at the reference density ρ_{ref}. Therefore, accurate prediction of the chemical potentials of the bulk and confined fluids is crucial to the development of an accurate CDFT approach. To validate the theoretical predictions for the chemical potential, the results of the homogeneous fluid theories are compared to those obtained from the grand canonical Monte Carlo simulations. In Fig. 1 (right plot), comparison is made for 6-mers between Monte Carlo simulation data and predictions from the FMSA based homogeneous fluid theory employing both the hard-sphere contact value and a contact value obtained from the exponential approximation (11). As can be seen from the figure, excellent agreement is obtained between the GCMC simulations and the FMSA with contact values obtained from the exponential approximation. When hard-sphere contact values are used the theory is not able to accurately predict the chemical potential, and, thus, as we will observe later, is not accurate in predicting the adsorption isotherms.

Radial density profiles of the monomers inside the pores obtained with the three theories considered (termed polymeric DFT, iSAFT DFT, and SCFT DFT) and Monte Carlo simulations are presented in Figs. 4 and 5, for 6-mers and 12-mers, respectively. To ease the comparison between the approaches, they were calculated at equal average packing fraction of the in-pore fluid. From the profiles, it is evident that the fluid is strongly depleted from the walls. When a flexible molecule is placed near a hard wall, the wall diminishes the number of possible conformations of the molecule, and because of that the molecule is entropically depleted from the wall. Similarly, the oligomers studied here are depleted from the pores, which is mainly because the pore walls decrease the number of possible conformations of the chain, and, additionally, due to the attraction between the monomers, which induces some energetic penalty on monomers close to walls. This depletion clearly manifests itself on the adsorption isotherms for the hard pores (see Figs. 2(a) and 3(a)), where the average densities of the adsorbed fluid are smaller than the corresponding bulk densities. Thus, in this regime, the process could be described as an intrusion[59] of a non-wetting fluid into a nanopore. As can be seen from the figures, polymeric DFT and iSAFT DFT are able to capture these depletion effects. However, the isotherms (Figs. 2 and 3) show that these two theories overestimate the amount of the adsorbed fluid, whereas the third approach that utilizes SCFT predicts more accurate behavior.

It is worth noting that depletion effects observed here are well known and were recognized decades ago.[60] The key quantity that governs the depletion is the free energy associated with the confinement of the chain, $\mathscr{F}_c$, which describes the partitioning of the chains between the bulk and the pore. The probability that the chain will enter the pore should scale as $\exp\{-\beta\mathscr{F}_c\}$.

From the profiles it is clear that the polymeric DFT approach, that uses only hard-sphere contact values, is the least accurate, underestimating the density near the wall and overestimating the density in the centre of the pore. Surprisingly, however, the density profiles predicted by the theory appear to be very accurate at the highest densities ($\eta_{pore} = 0.3$) studied. This is probably due to the density profiles being compared at equal pore packing fractions. If one examines the adsorption isotherms (see Figs. 4 and 5), it becomes clear that the theory with the hard-sphere contact value is completely inaccurate for the repulsive and moderately attractive pores, and only for the attractive pore is it able to qualitatively agree with the MC simulation results. This illustrates the need for a theory that not only predicts good structural properties within the pore, but also predicts the bulk and confined chemical potentials accurately.

The density profiles predicted by the other two theories are comparable in accuracy. The version of the polymeric DFT theory with exponential contact value is generally more accurate at the centre of the pore and less accurate near the pore walls. Conversely, for iSAFT DFT using the exponential contact value, the profiles are more accurate closer to the wall. Both polymeric DFT and iSAFT DFT overestimate the density of the fluid near the wall at higher densities (see $\eta_{pore} = 0.3$-profiles). Predictions from the SCFT DFT are very close to the results obtained from the polymeric DFT approach, which is probably because they both use the same expression for the free energy functional. There is however an important difference between them: specifically, the chain conformations sampled by the self-consistent field theory are self-avoiding, while for polymeric DFT (and iSAFT DFT) they are ideal.

Overall, all the CDFT approaches studied satisfactorily predict segment density profiles for the pores studied. The common problem is that they tend to be less accurate at higher densities (see Figs. 4(c), 4(f), 5(c), and 5(f)), where the theory with the hard-sphere contact value appears to give the best predictions. This suggests that the functional form used for the SW fluid contact value functional may require further refinement to correct these deficiencies. On the other hand, the adsorption isotherms can be successfully described only when the contact value contribution due to the SW attraction is taken into account (see Figs. 2 and 3), and does not seem to depend strongly on the particular functional form of the contact value functional.

As the pore walls become more attractive, the depletion of chains from the pore is balanced by the wall-fluid attraction. For the highest attraction of $\epsilon_{pore} = 2\epsilon$, the depletion is outweighed by the attraction and the pores become adsorbing, i.e., the density of the adsorbed fluid at small bulk densities is about two times that of the corresponding bulk fluid. The change of regimes from intrusion to adsorption, which is governed by the interplay between the depletion and attraction, is captured by the CDFT approaches studied. However, the isotherms predicted by the polymeric DFT and iSAFT DFT approaches generally tend to slightly overestimate the amount of the adsorbed fluid, while the SCFT provides better agreement with the simulation results. To explain this, we again note that the conformations of the chains sampled by the polymeric DFT and iSAFT DFT approaches are ideal, and, therefore, the particular configurations in which a chain intersects itself are not rejected. This artificially enlarges the number

of possible conformations of the chains inside the pore, and, as a result, the amount of the adsorbed fluid. Sampling self-avoiding chain conformations by the SCFT tends to significantly improve the agreement with the MC data, but for some cases (Fig. 3(b)) the discrepancies are still noticeable.

IV. CONCLUSIONS

The adsorption of oligomers of two different lengths (6 and 12 beads) into infinite narrow cylindrical pores was studied at supercritical temperature by employing several classical density functional theories (CDFT) and grand-canonical Monte Carlo simulation. The pores studied were sufficiently narrow to entropically deplete the oligomers. Additionally, the fluid-fluid attraction contributes to the depletion of the fluid, which for pores with purely hard walls results in an intrusive regime, in which adsorption is weak and the density of the adsorbed fluid is always lower than the corresponding density of the bulk fluid. Therefore, in order to accurately model the adsorption of the fluid, wall-fluid attraction was added in a form of the potential well near the hard wall. Capturing the interplay between the depletion and attraction was the main difficulty for the CDFT approaches studied. When exponential contact values are in place of the hard-sphere contact, the change from intrusive to adsorptive regimes is captured.

The examined CDFT approaches were based on the polymeric DFT theory of Yu and Wu,[48] the iSAFT DFT theory of Chapman and co-workers,[55,56] and SCFT DFT of Bryk and MacDowell.[57] To demonstrate the importance of an accurate underlying bulk homogeneous fluid theory, we examined two variants of polymeric DFT: one with exponential contact values for the reference fluid and one with hard-sphere contact values. The latter theory was demonstrated to be unable to reliably predict the chemical potential of the bulk fluid, and, consequently, the adsorption isotherms. It is, therefore, a requirement for the CDFT theories to be built upon an accurate homogeneous fluid theory and to employ accurate contact values in order to be quantitatively predictive.

Comparison between CDFTs based on iSAFT DFT and polymeric DFT, both using accurate exponential contact values, revealed that the two CDFT approaches provide similar performance for the prediction of density profiles and adsorption isotherms. However, due to the ideal/"non-self-avoiding" chain conformations sampled, the resulting adsorption isotherms overestimate the amount of the adsorbed fluid. The most accurate approach in this respect was SCFT, which samples more realistic chain conformations, and, in turn, is able to predict more accurate adsorption isotherms. This fact signifies the importance of the proper sampling of molecule conformations in order to develop predictive CDFTs.

ACKNOWLEDGMENTS

The authors acknowledge support from the Division of Chemical Sciences, Geosciences and Biosciences, Office of Basic Energy Sciences, U.S. Department of Energy.

APPENDIX: CONTACT VALUE AND DERIVATIVES

The FMSA contact-value correction reads

$$g_1(\eta) = \sum_{i=0}^{2} \left(A_i f_i^{(A)} + B_i f_i^{(B)} \right), \tag{A1}$$

where

$$A_i = -(1-\eta)^8 \frac{\left((\lambda+1)t_i^5 - t_i^4\right) e^{\lambda t_i}}{S_1^2(t_i)},$$

$$B_i = (1-\eta)^8 \left\{ \left[(\lambda+1)^2 S_1(t_i) - (\lambda+1) S_1(t_i) - (\lambda+1) S_2(t_i) \right] t_i^5 + \left[S_1(t_i) + S_2(t_i) + 4(\lambda+1) S_1(t_i) \right] t_i^4 - 4 S_1(t_i) t_i^3 \right\} e^{\lambda t_i} / S_1^3(t_i),$$

$$f_i^A = \left[-\frac{6t_i^5}{S^2(-t_i)} - \frac{2t_i^6 S_1(-t_i)}{S^3(-t_i)} \right] + \sum_{j=0}^{2} \left[-\frac{t_j^6 S_2(t_j)}{S_1^3(t_j)(t_i+t_j)^2} + \frac{4t_j^6 + 6t_i t_j^5}{S_1^2(t_j)(t_i+t_j)^3} \right],$$

$$f_i^B = \frac{t_i^6}{S_2(-t_i)} + \sum_{j=0}^{2} \left[-\frac{t_j^6 S_2(t_j)}{S_1^3(t_j)(t_i+t_j)} + \frac{5t_j^6 + 6t_i t_j^5}{S_1^2(t_j)(t_i+t_j)^2} \right],$$

$$L(t) = \left(1 + \frac{\eta}{2}\right) t + 1 + 2\eta,$$

$$S(t) = (1-\eta)^2 t^3 + 6\eta(1-\eta) t^2 + 18\eta^2 t - 12\eta(1+2\eta),$$

$$S_1(t) = 3(1-\eta)^2 t^2 + 12\eta(1-\eta) t + 18\eta^2,$$

$$S_2(t) = 6(1-\eta)^2 t + 12\eta(1-\eta).$$

In the above equations, $\eta = \pi\rho\sigma^3/6$ and t_j are roots of $S(t) = 0$ equation, and are given by

$$t_j = \frac{\left(-2\eta + (2\eta f)^{1/3}\left(y_+ c^j + y_- c^{-j}\right)\right)}{1-\eta}, \quad j = 0, 1, 2, \tag{A2}$$

where

$$f = 3 + 3\eta - \eta^2, \tag{A3}$$

$$y_\pm = \left(1 \pm \left(1 + \frac{2\eta^4}{f^2}\right)^{1/2}\right)^{1/3}, \tag{A4}$$

$$c = e^{2\pi i/3}, \quad with \quad i^2 = -1, \tag{A5}$$

and the derivatives of the roots read

$$\frac{\partial t_j}{\partial\rho} = \frac{\pi}{6}\left[\frac{t_j}{1-\eta} + \frac{1}{1-\eta}\left(-2 + \left(2f + 2\eta\frac{\partial f}{\partial\eta}\right)\right.\right.$$
$$\left.\left.\times\frac{y_+ c^j + y_- c^{-j}}{3(2\eta f)^{\frac{2}{3}}} + (2\eta f)^{\frac{1}{3}}\left(\frac{\partial y_+}{\partial\eta}c^j + \frac{\partial y_-}{\partial\eta}c^{-j}\right)\right)\right]. \tag{A6}$$

The derivative of the first-order correction of the contact value reads

$$\frac{\partial g_1}{\partial\rho} = \sum_{i=0}^{2}\left(\frac{\partial A_i}{\partial\rho}f_i^{(A)} + A_i\frac{\partial f_i^{(A)}}{\partial\rho} + \frac{\partial B_i}{\partial\rho}f_i^{(B)} + B_i\frac{\partial f_i^{(B)}}{\partial\rho}\right), \tag{A7}$$

where the corresponding derivatives of the coefficients could be calculated numerically, but, for the sake of completeness, we have presented them below:

$$\frac{\partial A_i}{\partial\rho} = \beta\varepsilon(1-\eta)^7\left[\frac{8\pi\sigma^3}{6}\frac{(\lambda+1)t_i^5 - t_i^4}{S_1^2(t_i)} - (1-\eta)\frac{5(\lambda+1)t_i^4 - 4t_i^3 + ((\lambda+1)t_i^5 - t_i^4)\lambda}{S_1^2(t_i)}\frac{\partial t_i}{\partial\rho}\right.$$
$$\left. + \frac{2(1-\eta)\left((\lambda+1)t_i^5 - t_i^4\right)}{S_1^3(t_i)}\left(S_2(t_i)\frac{\partial t_i}{\partial\rho} + \frac{\pi\sigma^3}{6}\frac{\partial S_1(t_i)}{\partial\eta}\right)\right]e^{\lambda t_i}, \tag{A8}$$

$$\frac{\partial B_i}{\partial\rho} = \beta\varepsilon\left[-\frac{8\pi\sigma^3}{6}\frac{(1-\eta)^7}{S_1(t_i)^3}\left(\left((\lambda+1)^2 S_1(t_i) - (\lambda+1)S_1(t_i) - (\lambda+1)S_2(t_i)\right)t_i^5\right.\right.$$
$$+ (S_1(t_i) + S_2(t_i) + 4(\lambda+1)S_1(t_i))t_i^4 - 4S_1(t_i)t_i^3\Big)e^{\lambda t_i}$$
$$+ \frac{(1-\eta)^8}{S_1(t_i)^3}\frac{\partial t_i}{\partial\rho}\left(((\lambda+1)^2 S_2(t_i) - (\lambda+1)S_2(t_i) - (\lambda+1)S_3)t_i^5\right.$$
$$+ 5((\lambda+1)^2 S_1(t_i) - (\lambda+1)S_1(t_i) - (\lambda+1)S_2(t_i))t_i^4 + (S_2(t_i) + S_3 + 4(\lambda+1)S_2(t_i))t_i^4$$
$$\left.+ 4(S_1(t_i) + S_2(t_i) + 4(\lambda+1)S_1(t_i))t_i^3 - 4S_2(t_i)t_i^3 - 12S_1(t_i)t_i^2\right)e^{\lambda t_i}$$
$$+ \frac{\pi\sigma^3}{6}\frac{(1-\eta)^8}{S_1(t_i)^3}\left(\left((\lambda+1)^2\frac{\partial S_1(t_i)}{\partial\eta} - (\lambda+1)\frac{\partial S_1(t_i)}{\partial\eta} - (\lambda+1)\frac{\partial S_2(t_i)}{\partial\eta}\right)t_i^5\right.$$
$$\left.\left. + \left(\frac{\partial S_1(t_i)}{\partial\eta} + \frac{\partial S_2(t_i)}{\partial\eta} + 4(\lambda+1)\frac{\partial S_1(t_i)}{\partial\eta}\right)t_i^4 - 4\frac{\partial S_1(t_i)}{\partial\eta}t_i^3\right)e^{\lambda t_i}\right]$$
$$+ \lambda B_i\frac{\partial t_i}{\partial\rho} - \frac{3B_i}{S_1(t_i)}\left(S_2(t_i)\frac{\partial t_i}{\partial\rho} + \frac{\pi\sigma^3}{6}\frac{\partial S_1(t_i)}{\partial\eta}\right), \tag{A9}$$

$$\frac{\partial f_i^A}{\partial\rho} = \left[\frac{\partial t_i}{\partial\rho}\left(-\frac{30t_i^4}{S^2(-t_i)} - \frac{12t_i^5 S_1(-t_i)}{S^3(-t_i)} - \frac{12t_i^5 S_1(-t_i) - 2t_i^6 S_2(-t_i)}{S^3(-t_i)} - \frac{6t_i^6 S_1(-t_i)^2}{S^4(-t_i)}\right)\right.$$
$$\left. + \frac{\pi\sigma^3}{6}\left(\frac{12t_i^5\frac{\partial S(-t_i)}{\partial\eta}}{S^3(-t_i)} - \frac{2t_i^6\frac{\partial S_1(-t_i)}{\partial\eta}}{S^3(-t_i)} + \frac{6t_i^6 S_1(-t_i)\frac{\partial S(-t_i)}{\partial\eta}}{S^4(-t_i)}\right)\right]$$
$$+ \sum_{j=0}^{2}\left[-\frac{\left(6t_j^5 S_2(t_j) + t_j^6 S_3\right)\frac{\partial t_j}{\partial\rho}}{\left(S_1^3(t_j)(t_i+t_j)^2\right)} + \frac{3t_j^6 S_2(t_j)^2\frac{\partial t_j}{\partial\rho}}{\left(S_1^4(t_j)(t_i+t_j)^2\right)} + \frac{2t_j^6 S_2(t_j)(\frac{\partial t_i}{\partial\rho} + \frac{\partial t_j}{\partial\rho})}{\left(S_1^3(t_j)(t_i+t_j)^3\right)}\right.$$
$$\left. + \frac{\left(24t_j^5 + 30t_i t_j^4\right)\frac{\partial t_j}{\partial\rho}}{\left(S_1^2(t_j)(t_i+t_j)^3\right)} + \frac{6t_j^5\frac{\partial t_i}{\partial\rho}}{\left(S_1^2(t_j)(t_i+t_j)^3\right)} - \frac{2\left(4t_j^6 + 6t_i t_j^5\right)S_2(t_j)\frac{\partial t_j}{\partial\rho}}{\left(S_1^3(t_j)(t_i+t_j)^3\right)}\right.$$

$$-3\frac{\left(4t_j^6+6t_it_j^5\right)\left(\frac{\partial t_j}{\partial\rho}+\frac{\partial t_i}{\partial\rho}\right)}{\left(S_1^2(t_j)(t_i+t_j)^4\right)}+\frac{\pi\sigma^3}{6}\left(-\frac{t_j^6\frac{\partial S_2(t_j)}{\partial\eta}}{S_1^3(t_j)(t_i+t_j)^2}+3\frac{t_j^6S_2(t_j)\frac{\partial S_1(t_j)}{\partial\eta}}{S_1^4(t_j)(t_i+t_j)^2}\right.$$
$$\left.-2\frac{\left(4t_j^6+6t_it_j^5\right)\frac{\partial S_1(t_j)}{\partial\eta}}{S_1^3(t_j)(t_i+t_j)^3}\right)\Bigg], \tag{A10}$$

$$\frac{\partial f_i^B}{\partial\rho}=\left[\frac{\partial t_i}{\partial\rho}\left(\frac{6t_i^5}{S(-t_i)^2}+\frac{2t_i^6S_1(-t_i)}{S(-t_i)^3}\right)-\frac{\pi\sigma^3}{6}\frac{2t_i^6}{S(-t_i)^3}\frac{\partial S(-t_i)}{\partial\eta}\right]$$
$$+\sum_{j=0}^{2}\left[-\frac{6t_j^5S_2(t_j)+t_j^6S_3(t_i)}{S_1(t_j)^3(t_i+t_j)}\frac{\partial t_j}{\partial\rho}+\frac{3t_j^6S_2(t_j)^2}{S_1(t_j)^4(t_i+t_j)}\frac{\partial t_j}{\partial\rho}\right.$$
$$+\frac{t_j^6S_2(t_j)}{S_1(t_j)^3(t_i+t_j)^2}\left(\frac{\partial t_i}{\partial\rho}+\frac{\partial t_j}{\partial\rho}\right)+\frac{30t_j^5+30t_it_j^4}{S_1(t_j)^2(t_i+t_j)^2}\frac{\partial t_j}{\partial\rho}$$
$$+\frac{6t_j^5}{S_1(t_j)^2(t_i+t_j)^2}\frac{\partial t_i}{\partial\rho}-\frac{2(5t_j^6+6t_it_j^5)S_2(t_j)}{S_1(t_j)^3(t_i+t_j)^2}\frac{\partial t_j}{\partial\rho}$$
$$-\frac{2(5t_j^6+6t_it_j^5)}{S_1(t_j)^2(t_i+t_j)^3}\left(\frac{\partial t_j}{\partial\rho}+\frac{\partial t_i}{\partial\rho}\right)+\frac{\pi\sigma^3}{6}\left(-\frac{t_j^6}{S_1(t_j)^3(t_i+t_j)}\frac{\partial S_2(t_j)}{\partial\eta}\right.$$
$$\left.\left.+\frac{3t_j^6S_2(t_j)}{S_1(t_j)^4(t_i+t_j)}\frac{\partial S_1(t_j)}{\partial\eta}-\frac{2(5t_j^6+6t_it_j^5}{(S_1(t_j)^3(t_i+t_j)^2}\frac{\partial S_1(t_j)}{\partial\eta}\right)\right]. \tag{A11}$$

[1] M. N. K. Ishizaki and S. Komarneni, *Porous Materials: Process Technology and Applications* (Chapman and Hall, 1998), Vol. 4.
[2] M. Mulder, *Basic Principles of Membrane Technology* (Springer, 1996).
[3] A. Basile and F. Gallucci, *Membranes for Membrane Reactors: Preparation, Optimization and Selection* (Wiley, 2011).
[4] J. C. Janson, *Protein Purification: Principles, High Resolution Methods, and Applications* (Wiley, 2011).
[5] K. Gubbins, Y. Liu, J. Moore, and J. Palmer, Phys. Chem. Chem. Phys. **13**, 58 (2011).
[6] J. Wu, AIChE J. **52**, 1169 (2006).
[7] L. Frink and A. Salinger, J. Chem. Phys. **110**, 5969 (1999).
[8] L. Frink and A. Salinger, J. Comput. Phys. **159**, 407 (2000).
[9] L. Frink and A. Salinger, J. Comput. Phys. **159**, 425 (2000).
[10] M. Sears and L. Frink, J. Comput. Phys. **190**, 184 (2003).
[11] S. Hlushak, W. Rżysko, and S. Sokołowski, J. Chem. Phys. **131**, 094904 (2009).
[12] M. G. Knepley, D. A. Karpeev, S. Davidovits, R. S. Eisenberg, and D. Gillespie, J. Chem. Phys. **132**, 124101 (2010).
[13] M. Levesque, R. Vuilleumier, and D. Borgis, J. Chem. Phys. **137**, 034115 (2012).
[14] S. Hlushak, C. McCabe, and P. Cummings, J. Chem. Phys. **137**, 104104 (2012).
[15] M. Levesque, V. Marry, B. Rotenberg, G. Jeanmairet, R. Vuilleumier, and D. Borgis, J. Chem. Phys. **137**, 224107 (2012).
[16] X. Wang, J. Mi, and C. Zhong, J. Chem. Phys. **138**, 164704 (2013).
[17] Y. Liu, S. Zhao, and J. Wu, J. Chem. Theory Comput. **9**, 1896 (2013).
[18] M. Borówko, T. Pöschel, S. Sokolowski, and T. Staszewski, J. Phys. Chem. B **117**, 1166 (2013).
[19] Y. Rosenfeld, Phys. Rev. Lett. **63**, 980 (1989).
[20] R. Roth, R. Evans, A. Lang, and G. Kahl, J. Phys.: Condens. Matter **14**, 12063 (2002).
[21] H. Hansen-Goos and R. Roth, J. Phys.: Condens. Matter **18**, 8413 (2006).
[22] Y. Tang, J. Chem. Phys. **127**, 164504 (2007).
[23] S. Hlushak, A. Trokhymchuk, and S. Sokołowski, J. Chem. Phys. **130**, 234511 (2009).
[24] S. Hlushak, A. Trokhymchuk, and S. Sokołowski, J. Chem. Phys. **134**, 114101 (2011).
[25] Y. Tang and B. Lu, J. Chem. Phys. **99**, 9828 (1993).
[26] J. Lebowitz and J. Percus, Phys. Rev. **144**, 251 (1966).
[27] M. Wertheim, J. Chem. Phys. **55**, 4291 (1971).
[28] E. Waisman and J. L. Lebowitz, J. Chem. Phys. **56**, 3086 (1972).
[29] H. C. Andersen and D. Chandler, J. Chem. Phys. **57**, 1918 (1972).
[30] R. Palmer and J. Weeks, J. Chem. Phys. **58**, 4171 (1973).
[31] S. Adelman and J. Deutch, J. Chem. Phys. **59**, 3971 (1973).
[32] L. Blum, Mol. Phys. **30**, 1529 (1975).
[33] Y. Tang and B. Lu, J. Chem. Phys. **100**, 6665 (1994).
[34] Y. Tang and B. Lu, J. Chem. Phys. **100**, 3079 (1994).
[35] S. Hlushak, P. Hlushak, and A. Trokhymchuk, J. Chem. Phys. **138**, 164107 (2013).
[36] Y. Tang, Y. Lin, and Y. Li, J. Chem. Phys. **122**, 184505 (2005).
[37] S. Hlushak and A. Trokhymchuk, Condens. Matter Phys. **15**, 23003 (2012).
[38] Y. Tang, J. Chem. Phys. **118**, 4140 (2003).
[39] E.-Y. Kim, S.-C. Kim, and B.-S. Seong, Fluid Phase Equilib. **308**, 90 (2011).
[40] Z. Jin, Y. Tang, and J. Wu, J. Chem. Phys. **134**, 174702 (2011).
[41] S. Zong-Li, K. Yan-Shuang, K. Yan-Mei, L. Zhi-Cheng, and M. Heng-Xin, Chin. Phys. B **21**, 066103 (2012).
[42] A. Gallardo, S. Grandner, N. G. Almarza, and S. H. Klapp, J. Chem. Phys. **137**, 014702 (2012).
[43] D. Zhou, J. Mi, and C. Zhong, J. Phys. Chem. C **116**, 3042 (2012).
[44] S. Zong-Li and K. Yan-Shuang, Chin. Phys. Lett. **28**, 026101 (2011).
[45] E.-Y. Kim, S.-C. Kim, and S.-H. Suh, Phys. Rev. E **85**, 051203 (2012).
[46] S.-C. Kim, S.-H. Suh, and B.-S. Seong, J. Chem. Phys. **137**, 114703 (2012).
[47] S. Hlushak, A. Trokhymchuk, and I. Nezbeda, Condens. Matter Phys. **14**, 33004 (2011).
[48] Y. Yu and J. Wu, J. Chem. Phys. **117**, 2368 (2002).
[49] M. Wertheim, J. Chem. Phys. **87**, 7323 (1987).
[50] Y. Yu and J. Wu, J. Chem. Phys. **117**, 10156 (2002).
[51] F. Tavares, J. Chang, and S. Sandler, Mol. Phys. **86**, 1451 (1995).
[52] D. Chandler, J. D. McCoy, and S. J. Singer, J. Chem. Phys. **85**, 5971 (1986).
[53] D. Chandler, J. D. McCoy, and S. J. Singer, J. Chem. Phys. **85**, 5977 (1986).

[54]D. Gillespie, W. Nonner, and R. Eisenberg, Phys. Rev. E **68**, 031503 (2003).
[55]S. Tripathi and W. Chapman, J. Chem. Phys. **122**, 094506 (2005).
[56]S. Jain, A. Dominik, and W. G. Chapman, J. Chem. Phys. **127**, 244904 (2007).
[57]P. Bryk and L. MacDowell, J. Chem. Phys. **129**, 104901 (2008).
[58]D. Frenkel and B. Smit, *Understanding Molecular Simulation: From Algorithms to Applications* (Academic Press, 2001), Vol. 1.
[59]B. Coasne, A. Galarneau, R. J. Pellenq, and F. Di Renzo, Chem. Soc. Rev. **42**, 4141 (2013).
[60]P. G. De Gennes, *Scaling Concepts in Polymer Physics* (Cornell University Press, 1979).